

# Pulsed mid-IR $\text{Cr}^{2+} : \text{ZnS}$ and $\text{Cr}^{2+} : \text{ZnSe}$ lasers pumped by Raman-shifted $Q$ -switched neodymium lasers

K. Graham, V.V. Fedorov, S.B. Mirov, M.E. Doroshenko,  
T.T. Basiev, Yu.V. Orlovskii, V.V. Osiko, V.V. Badikov, V.L. Panyutin

**Abstract.** The spectral and lasing properties of  $\text{Cr}^{2+} : \text{ZnS}$  and  $\text{Cr}^{2+} : \text{ZnSe}$  crystals pumped by Raman-shifted nanosecond neodymium lasers are studied. Tunable pulsed lasing is obtained in the mid-IR range between 2.05 and 2.40  $\mu\text{m}$ . The minimum lasing threshold was 170  $\mu\text{J}$  at the maximum slope efficiency of 20%.

**Keywords:** IR lasers, tunable lasers, optical pump.

## 1. Introduction

The development of compact tunable mid-IR lasers operating at room temperature is of great interest for many scientific studies and applications. Such lasers can be used in medicine, environmental control and spectroscopic investigations. In this connection, chalcogenide crystals doped with transition-metal ions, in particular,  $\text{Cr}^{2+}$  ions attract special interest. The fundamental properties of impurity  $\text{Cr}^{2+}$  ions in II–VI semiconductors have been studied since the 1970s [1–5]. The models describing the symmetry of these optical centres and the splitting of levels of the  $\text{Cr}^{2+}$  ion in a crystal tetragonal field have been proposed in Refs [2–6]. A new wave of investigations of these materials was initiated in papers [7–9], where it was proposed to use them in solid-state tunable mid-IR lasers. Room-temperature lasing has been obtained at the  ${}^5E \rightarrow {}^5T_2$  transitions of  $\text{Cr}^{3+}$  ions in the ZnS [7, 8, 10–13], ZnSe [7, 8], CdSe [14], and  $\text{Cd}_{1-x}\text{Mn}_x\text{Te}$  [15–17] crystals in the wavelength range from 2 to 3  $\mu\text{m}$ . Continuous-wave [18–21], pulsed [22, 10] and mode-locked [23–25] lasing has been achieved. The crystals were pumped both by flashlamps and laser diodes [26–28]. The ZnS and ZnSe crystals have the best physical properties among the II–VI crystals. They are nonhygroscopic (the solubility of ZnS and ZnSe in water is less than 0.01), their thermal

conductivity is higher than that for other crystals of this type (27  $\text{W m}^{-1} \text{K}^{-1}$  for ZnS and 19  $\text{W m}^{-1} \text{K}^{-1}$  for ZnSe), and their temperature derivative of the refractive index is smaller than in other crystals of this type (as  $46 \times 10^{-6} \text{K}^{-1}$  for ZnS and  $70 \times 10^{-6} \text{K}^{-1}$  for ZnSe [29]). One of the problems in the development of  $\text{Cr}^{2+} : \text{ZnS}$  and  $\text{Cr}^{2+} : \text{ZnSe}$  lasers is the synthesis of crystals with a homogeneous distribution of impurity chromium ions at high concentrations and low passive losses. In this connection it is interesting to dope preliminary grown pure crystals with impurities by the method of thermal diffusion. This method offers an advantage of the independent optimisation of the growth of high-quality crystals and the diffusion of impurity ions. In addition, this technology allows one to control the impurity concentration by changing the temperature and duration of thermal diffusion during doping.

Neodymium lasers can be used as one of the pump sources for high-power pulsed  $\text{Cr}^{2+} : \text{ZnS}$  and  $\text{Cr}^{2+} : \text{ZnSe}$  lasers. These lasers are widely used, optimised for high-power diode pump, and can be easily scaled to obtain the required output pulse energy.

In this paper, we studied the spectral properties of  $\text{Cr}^{2+} : \text{ZnS}$  and  $\text{Cr}^{2+} : \text{ZnSe}$  crystals grown by the method of chemical transport followed by diffusion doping with chromium ions, as well as their laser parameters upon pumping by nanosecond pulses. As a base radiation source for spectroscopic studies and pumping of the crystals, we used  $Q$ -switched neodymium lasers. The output radiation from a 1.064- $\mu\text{m}$  neodymium laser was converted with the help of stimulated Raman scattering (SRS) in a cell with deuterium or hydrogen to radiation at 1.56 or 1.907  $\mu\text{m}$  lying within the absorption band of  $\text{Cr}^{2+} : \text{ZnS}$  or  $\text{Cr}^{2+} : \text{ZnSe}$  crystals, respectively. In addition, we also used for pumping the 1.33–1.34- $\mu\text{m}$  radiation from  $\text{Nd}^{3+} : \text{YAG}$  and  $\text{Nd}^{3+} : \text{Cr}^{2+} : \text{GGG}$  lasers shifted by SRS in  $\text{BaWO}_4$  crystals.

## 2. Synthesis of crystals

The ZnS and ZnSe crystals were grown by the method of chemical transport [3] from a vapour phase in a quartz ampoule of diameter 20 mm and length 200 mm using iodine transport. The difference of temperatures in the mixture and crystallisation zones was approximately 100  $^\circ\text{C}$ . The concentration of  $\text{I}_2$  during the crystal growth was 2–5  $\text{mg cm}^{-3}$ . Unoriented ZnS and ZnSe crystal samples of size 2  $\times$  2  $\times$  1 cm had the hexagonal structure. Plates of size 5  $\times$  5 mm and thickness 1–5 mm were manufactured from

K. Graham, S.B. Mirov University of Alabama at Birmingham, 1300 University Blvd., Birmingham, AL 35294-1170, USA;

V.V. Fedorov, M.E. Doroshenko, T.T. Basiev, Yu.V. Orlovskii,  
V.V. Osiko A.M. Prokhorov General Physics Institute, Russian Academy of Sciences, ul. Vavilova 38, 119991 Moscow, Russia;  
e-mail: basiev@lst.gpi.ru;

V.V. Badikov, V.L. Panyutin Kubanskii State University,  
ul. Stavropol'skaya 142, 350040 Krasnodar, Russia

Received 23 June 2003

Kvantovaya Elektronika 34 (1) 8–14 (2004)

Translated by M.N. Sapozhnikov

the samples. Chromium was doped into ZnS (ZnSe) crystals by thermal diffusion. The working surfaces of the plates were preliminary polished.

The plates were placed together with the CrS (CrSe) powder (providing the molar concentration of chromium of 0.1 % – 1.0 % in a final sample) into a quartz ampoule. The ampoule was pumped to  $2 \times 10^{-5}$  Torr and sealed off. Ampoules prepared this way were placed into an oven for annealing. The annealing time was varied from 14 to 40 days, while the annealing temperature was changed from 820 to 1120 °C. After the annealing, the working surfaces of the plates were subjected to fine polishing. Along with samples prepared by the thermal diffusion method, we fabricated samples doped with chromium from a metal film deposited on the surface of single crystal plates. The chromium film was prepared on samples by the method of pulsed laser deposition in a vacuum chamber, and then the crystals were placed into quartz ampoules. The ampoules were pumped to  $10^{-5}$  Torr and annealed at 1000 °C for ten days.

### 3. Spectral properties of Cr<sup>2+</sup> : ZnS and Cr<sup>2+</sup> : ZnSe laser crystals

According to the Hund rule, the ground state of free Cr<sup>2+</sup> ( $3d^4$ ) ions is the  ${}^5D$  state with the total degeneracy multiplicity equal to  $g({}^5D) = (2S + 1)(2L + 1) = 25$ . This state of Cr<sup>2+</sup> ions is split in a weak tetragonal  $T_d$  crystal field into the ground  ${}^5T_2$  and excited  ${}^5E$  states [2, 4], with the ratio of the degeneracy multiplicities equal to  $g({}^5E)/g({}^5T_2) = 2/3$ . The wavelengths of the  ${}^5T_2 \leftrightarrow {}^5E$  transitions in Cr<sup>2+</sup> ions in chalcogenide crystals lie in the range from 2 to 4  $\mu\text{m}$ . These transitions are spin-allowed transitions. The rest of the transitions from the excited  ${}^5E$  state in Cr<sup>2+</sup> ions are forbidden according to the spin selection rule. As a result, the excited-state absorption is absent, making Cr<sup>2+</sup>-doped chalcogenide crystals promising laser media for the mid-IR range [7, 8]. The EPR studies showed that the ground-state symmetry of Cr<sup>2+</sup> ions is perturbed along the (001) crystal axis. It has been shown in Ref. [2] that this perturbation can be caused by the static Jahn–Teller effect. In this case, the local symmetry of Cr<sup>2+</sup> ions is reduced to  $D_{2d}$  [2, 4, 5]. Such a perturbation leads to the splitting of the ground and excited states into the sublevels  ${}^5E \rightarrow {}^5\hat{A}_1 + {}^5\hat{B}_1$  and  ${}^5T_2 \rightarrow {}^5\hat{B}_2 + {}^5\hat{E}_2$  (the symbol  $\hat{\phantom{x}}$  denotes irreducible representations). In this case, the ratio of the degeneracy multiplicities for levels are  $g({}^5\hat{A}_1)/g({}^5\hat{B}_1) = 1$  and  $g({}^5\hat{B}_2)/g({}^5\hat{E}_2) = 1/2$ . The  ${}^5\hat{B}_2({}^5T_2) \rightarrow {}^5\hat{E}_2({}^5E)$  transition in ZnS and ZnSe crystals corresponds to a broad absorption band in the range from 700 to 3000  $\text{cm}^{-1}$ . The parameters of the Jahn–Teller perturbation for Cr<sup>2+</sup> ions in ZnS and ZnSe crystals are  $E_{JT}({}^5E) \approx 50 \text{ cm}^{-1}$  and  $E_{JT}({}^5T_2) \approx 350 \text{ cm}^{-1}$  [2, 4, 5]. The degeneracy of the levels is further removed due to the spin-spin and spin-orbit interactions. The splitting of the  ${}^5\hat{B}_2$  ground-state levels in ZnS and ZnSe crystals is approximately 7  $\text{cm}^{-1}$ . However, a dynamic model for perturbation of Cr<sup>2+</sup> ions in a tetragonal crystal field was proposed in some papers (see, for example, Ref. [6]). According to this model, the  $T_d$  symmetry is preserved, and the level splitting is much smaller, being only a few inverse centimetres. As a result, the room-temperature populations of the sublevels of the ground and excited states can be assumed identical. The energy level diagrams

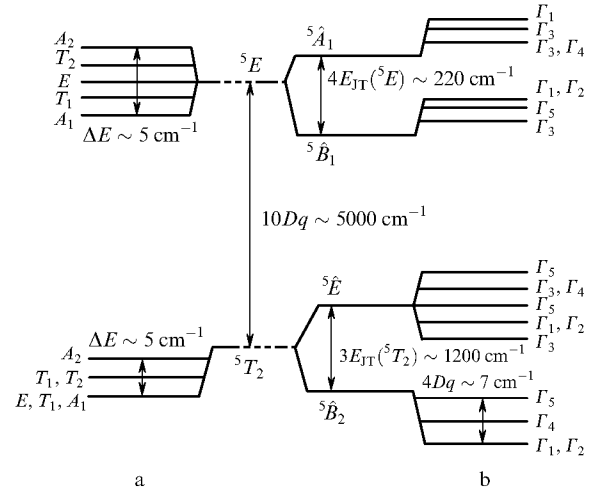
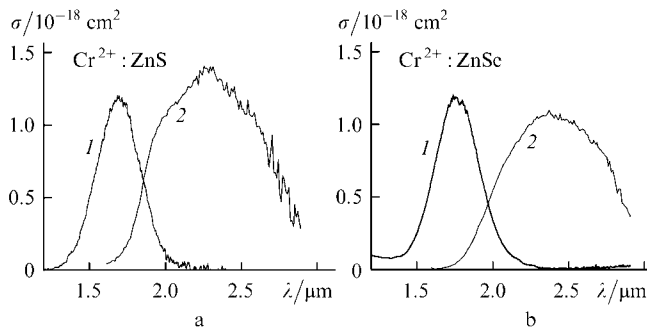


**Figure 1.** Energy level diagrams for Cr<sup>2+</sup> ions in a crystal field of the symmetry  $T_d$  in the case of perturbation produced by the dynamic Jahn–Teller effect [5, 6] (a) and in a crystal field of the symmetry  $D_{2d}$  in the case of perturbation produced by the static Jahn–Teller effect [2, 5] (b).

corresponding to the two splitting models considered above are presented in Fig. 1.

We studied the absorption and luminescence spectra corresponding to the  ${}^5T_2 \leftrightarrow {}^5E$  transitions in the temperature range from 14 to 450 K. The luminescence spectra were recorded with an Acton Research ARC-300i spectrometer. Luminescence was excited by a cw erbium-doped fibre laser (ELD-2, IPG Photonics). The luminescence emission was modulated with a mechanical shutter at a frequency of 800 Hz and measured with a PbS detector using a lock-in amplifier. The spectral sensitivity of the detection system was calibrated using an Oriel 9-2050 tungsten halogen lamp. It was shown [2] that the absorption coefficient  $\alpha$  (in  $\text{cm}^{-1}$ ) of a Cr<sup>2+</sup> : ZnSe crystal at the Cr<sup>2+</sup> concentration of no more than  $4 \times 10^{19} \text{ cm}^{-3}$  at room temperature at the frequency 5650  $\text{cm}^{-1}$  is proportional to the concentration of chromium ions  $n_{\text{Cr}}$  (in  $\text{cm}^{-3}$ ):  $\alpha \approx 1.2 \times 10^{-18} n_{\text{Cr}}$ . This result is close to that obtained in Ref. [31], where the absorption cross section was measured by the saturation of the crystal transmission upon pulsed excitation. Approximately the same absorption coefficient at the maximum of the absorption spectrum can be obtained for a Cr<sup>2+</sup> : ZnS crystal using the data from Ref. [3]. The room-temperature absorption spectra of samples recorded with a Shimadzu-UV3101PC spectrophotometer are presented in Fig. 2.

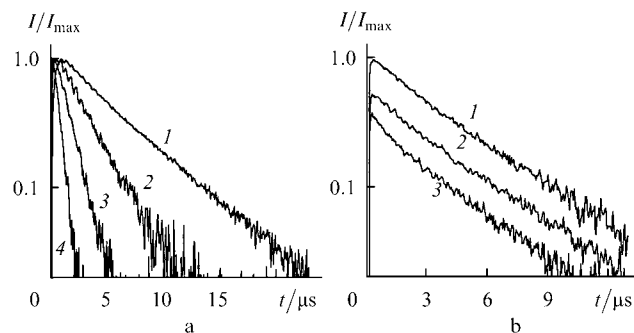
The luminescence kinetics of Cr<sup>2+</sup> ions was studied by exciting them by 5-ns pulses from a neodymium laser whose radiation was frequency-shifted to 1.56 or 1.907  $\mu\text{m}$  due to SRS in deuterium or hydrogen. The luminescence emission was detected with an InSb detector with the time resolution of 0.5  $\mu\text{s}$ . Figure 3b shows the room-temperature luminescence kinetics measured at several wavelengths in a Cr<sup>2+</sup> : ZnS crystal ( $n_{\text{Cr}} \approx 3 \times 10^{18} \text{ cm}^{-3}$ ). The luminescence decay curves measured at different wavelengths are well described within the experimental error by single exponential with the decay time  $\tau = 4.3 \mu\text{s}$  (a slight deviation from an exponential decay of luminescence at a wavelength of 2.25  $\mu\text{m}$  is caused by scattered laser radiation detected at the long-wavelength edge of the luminescence spectrum).



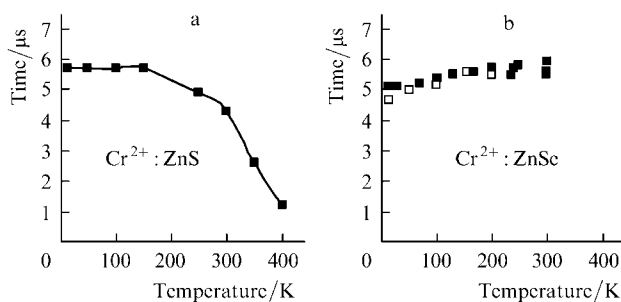
**Figure 2.** Absorption (1) and luminescence (2) cross sections for the  ${}^5T_2 \leftrightarrow {}^5E$  transitions in  $\text{Cr}^{2+}$  ions in ZnS (a) and ZnSe (b) crystals at room temperature.

Figure 3a demonstrates the luminescence decay at 1.95  $\mu\text{m}$  detected for a  $\text{Cr}^{2+}:\text{ZnS}$  crystal at different temperatures. The decay time  $\tau$  of luminescence increases up to 5.7  $\mu\text{s}$  with decreasing the crystal temperature down to 14 K. Figure 4 shows the temperature dependences of the excited-state lifetimes of  $\text{Cr}^{2+}$  ions in ZnS and ZnSe crystals. One can see that the excited-state lifetime slightly changes in the temperature range from 14 to 300 K.

The luminescence lifetimes of  $\text{Cr}^{2+}$  ions in a ZnS crystal at room temperature are close to the values 4.7–5.4  $\mu\text{s}$  obtained in Ref. [4], but shorter than the lifetime 8  $\mu\text{s}$  measured in Ref. [7]. This is probably explained by the influence of reabsorption. Another reason can be the



**Figure 3.** Decay of luminescence of  $\text{Cr}^{2+}$  ions at 1.95  $\mu\text{m}$  in ZnS crystals excited by 5-ns, 1.56- $\mu\text{m}$  pulses from the  $D_2$  Raman laser at temperatures 14 (1), 352 (2) and 401 K (3) (a), as well as at the wavelengths 1.95 (1), 2.15 (2), and 2.25  $\mu\text{m}$  (3) at 300 K (b). Curve (4) is the time resolution of the detection system upon registration at the pump wavelength.



**Figure 4.** Dependences of the decay time of luminescence of  $\text{Cr}^{2+}$  ions in the ZnS (a) and ZnSe (b) crystals upon pulsed excitation at 1.56 ( $\blacksquare$ ) and 1.907  $\mu\text{m}$  ( $\square$ ).

dependence of the transition oscillator strength on the crystal growth technology (in Ref. [7], crystals were grown by the physical transport method). We observed a slight increase in the luminescence lifetime for a  $\text{Cr}^{2+}:\text{ZnSe}$  crystal with temperature. This can be explained by a lower probability of radiative transitions from the higher-lying components  $\Gamma_1$ ,  $\Gamma_3$ ,  $\Gamma_4$ , and  ${}^5A_1$  (Fig. 1) of the excited state or by a slight variation in the lifetime of excited centres within the inhomogeneous luminescence band.

The concentration quenching of luminescence of a  $\text{Cr}^{2+}:\text{ZnSe}$  crystal was studied in detail in Ref. [32], where it was shown that it can be neglected at room temperature for concentrations below  $10^{19} \text{cm}^{-3}$ . However, the excited-state lifetime drastically decreases at higher concentrations. The data presented in Fig. 4 allow us to estimate the quantum yield of luminescence as the ratio of the luminescence lifetime measured at room temperature to the radiative lifetime. The latter was assumed equal to the maximum luminescence decay time measured in the temperature range from 14 to 450 K. The quantum yield of luminescence of chromium ions in ZnS and ZnSe crystals found by this method was 0.75 and  $\sim 1$ , respectively.

We also studied the dependence of the luminescence intensity of  $\text{Cr}^{2+}:\text{ZnS}$  crystals on the polarisation of exciting radiation. The luminescence intensity was measured in these experiments along the pump beam direction and perpendicular to it. However, the difference in the luminescence intensities did not exceed the experimental error ( $\sim 8\%$ ). The absorption cross section for the  ${}^5T_2 \leftrightarrow {}^5E$  transition of  $\text{Cr}^{2+}$  ions in ZnS (ZnSe) crystals (Fig. 2) was calculated from the calibrated luminescence spectrum using the relation [33]

$$\sigma_{\text{em}}(\lambda) = \frac{\lambda^5 I(\lambda)}{8\pi c n^2 \tau_{\text{rad}} \int \lambda I(\lambda) d\lambda}, \quad (1)$$

where the refractive index is  $n = 2.27$  (2.44); the radiative lifetime is  $\tau_{\text{rad}} = 6 \mu\text{s}$  (6  $\mu\text{s}$ ); and  $I(\lambda)$  is the spectral intensity distribution measured in  $\text{W m}^{-2} \text{nm}^{-1}$ .

The luminescence cross sections for  $\text{Cr}^{2+}:\text{ZnS}$  and  $\text{Cr}^{2+}:\text{ZnSe}$  crystals calculated in this way in the maximum of the gain curve were  $1.4 \times 10^{-18}$  and  $1 \times 10^{-18} \text{cm}^2$ , respectively. The spectral dependences coincide with data reported in [7]; however, the absolute values of the radiative lifetime differ from the values  $\tau_{\text{rad}} = 11$  and 8  $\mu\text{s}$  obtained for  $\text{Cr}^{2+}:\text{ZnS}$  and  $\text{Cr}^{2+}:\text{ZnSe}$  crystals in [7].

#### 4. Lasing experiments

The first series of experiments on tunable lasing was performed with a  $\text{Cr}^{2+}:\text{ZnS}$  crystal, which was pumped by radiation from a  $\text{Nd}^{3+}:\text{YAG}$  laser Raman shifted in a cell with deuterium. The scheme of the experiment is shown in Fig. 5. The Raman converter was pumped by 5-ns, 1.064- $\mu\text{m}$  pulses from a single-frequency  $\text{Nd}^{3+}:\text{YAG}$  laser. An optical isolator placed between the laser and the SRS cell prevented the damage of active elements by backward radiation scattered in the cell. The 1.56- $\mu\text{m}$  backscattered radiation pulses with energy of up to 100 mJ were attenuated and focused into a  $\text{Cr}^{2+}:\text{ZnS}$  crystal with a lens of the focal length 26.5 cm. The stability of the pump energy was approximately 5%. A semispherical resonator of length 18.5 cm was formed by a flat dichroic mirror deposited on the active-element face and by a spherical

mirror with radius of curvature  $\rho = 20$  cm. The second face of the crystal was covered by an anti-reflection coating for the lasing wavelength range and by a highly reflecting coating for the pump wavelength, providing the double-pass pumping in the active element.

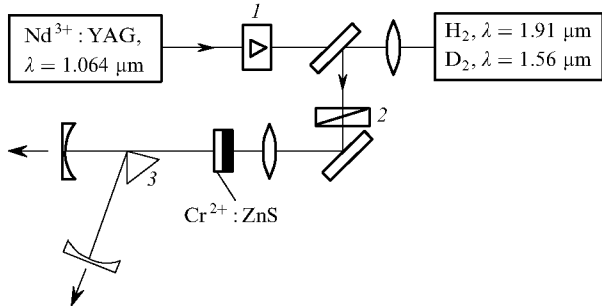


**Figure 5.** Experimental setup for studying the Cr<sup>2+</sup> : ZnS laser pumped by radiation from the Nd<sup>3+</sup> : YAG laser frequency-shifted due to SRS in a hydrogen or deuterium cell: (1) optical isolator; (2) attenuator; (3) CaF<sub>2</sub> prism.

The averaged absorption coefficient in the 1.7-mm thick active element was  $\sim 3.5$  cm<sup>-1</sup>. However, the distribution of chromium ions over the crystal depth was strongly inhomogeneous. The output mirror had transmission of 10 % or 20 % in the spectral range between 2.05 and 2.5  $\mu$ m and 25 % at the pump wavelength. The calculated waist of the resonator mode was 200  $\mu$ m. The output emission was separated from pump radiation using a Ge filter.

Figure 6 shows the dependence of the output energy on the absorbed pump energy for the output-mirror transmission  $T = 10$  %. One can see that the lasing threshold is achieved at the pump energy  $E_{th1} = 170$   $\mu$ J and the slope efficiency is 20 %. The spectral width of the laser pulse was 90 nm. The maximum output energy was limited by the optical damage of the active-element coatings. For the output mirror with  $T = 20$  %, the lasing threshold was  $E_{th2} = 250$   $\mu$ J. The passive losses at the lasing wavelength per one round-trip were estimated to be  $\sim 14$  % using the relation [33]

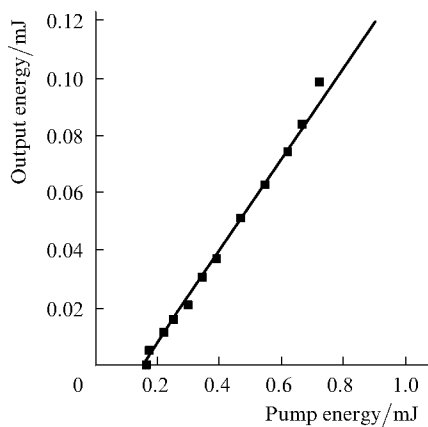


**Figure 6.** Output energy of the Cr<sup>2+</sup> : ZnS laser with the output-mirror reflectivity  $R = 90$  %.

$$L_p = \frac{E_{th1} \ln R_1 - E_{th2} \ln R_2}{E_{th1} - E_{th2}}, \quad (2)$$

where  $R_1$  and  $R_2$  are the reflectivities of output mirrors.

To obtain tunable output radiation, we placed a CaF<sub>2</sub> prism into the resonator at a distance of 7 cm from the output mirror (with the reflectivity  $R = 90$  %). The insertion of the prism into the resonator increased the lasing threshold up to 240  $\mu$ J. Figure 7 shows the spectrum of tunable laser output in the range between 2.05 and 2.40  $\mu$ m obtained at the three-fold excess of pump radiation over the lasing threshold. The maximum of the tuning curve is located at 2.25  $\mu$ m. The tuning range in the long-wavelength region was limited by the mirror coatings, whose reflectivities decreased at long wavelengths.

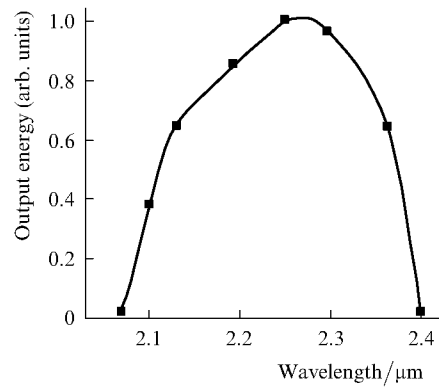


**Figure 7.** Output tuning curve for the Cr<sup>2+</sup> : ZnS laser with the output-mirror reflectivity  $R = 90$  % and a CaF<sub>2</sub> prism used for tuning.

In the second series of experiments, we used an acousto-optically  $Q$ -switched Nd<sup>3+</sup> : YAG laser as a base pumping source, which emitted 40–50-ns, 1.34- $\mu$ m pulses. This laser was used to pump a Raman laser based on a BaWO<sub>4</sub> crystal of length 42 mm (Fig. 8). This crystal was chosen as an active medium for a solid-state IR Raman laser due to its unique properties [34, 35]. The BaWO<sub>4</sub> crystal provides a high peak intensity of Raman scattering, which is very close to its record value in a Ba(NO<sub>3</sub>)<sub>2</sub> crystal, but unlike the latter, this crystal is nonhygroscopic, hard, and has a high thermal conductivity, while its absorption spectrum is shifted to the IR region, allowing one to obtain SRS in the range between 1.7 and 3  $\mu$ m. The resonator of the Raman laser was formed by two flat mirrors. The reflectivity of the input mirror was  $R = 90$  % – 100 % in the range from

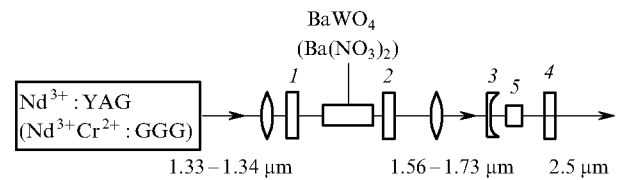


**Figure 8.** Experimental setup for studying the Cr<sup>2+</sup> : ZnS laser pumped by radiation from a neodymium laser frequency-shifted due to SRS in BaWO<sub>4</sub> and Ba(NO<sub>3</sub>)<sub>2</sub> crystals; (1, 2) input and output mirrors of the Raman laser; (3, 4) input and output mirrors of the laser under study; (5) active element.

1.5 to 2.0  $\mu\text{m}$  and its transmission was  $T = 80\% - 90\%$  at the pump wavelength 1.34  $\mu\text{m}$ . The output mirror had  $R = 50\%$  at 1.53  $\mu\text{m}$  and  $T = 14\%$  at 1.78  $\mu\text{m}$ . To avoid the optical damage of the crystal, the pump radiation was focused by a lens with the focal distance  $f = 180$  mm into a spot at a distance of a few millimetres in front of the input face of the crystal.

Figure 9a shows the general output emission spectrum of the laser. One can see that even when the output mirror with  $R = 50\%$  at the wavelength corresponding to the first Stokes component ( $\lambda = 1.53$   $\mu\text{m}$ ,  $\Delta\nu = 925$   $\text{cm}^{-1}$ ) was used, lasing was obtained at the wavelengths 1.78 and 2.13  $\mu\text{m}$  corresponding to the second and third Stokes components. An additional weak scattering observed near the first Stokes component is caused by another, weaker vibrational mode ( $\Delta\nu = 332$   $\text{cm}^{-1}$ ) observed in the spontaneous Raman spectrum of the  $\text{BaWO}_4$  crystal. The output parameters of the Raman laser are presented in Fig. 9b. The conversion efficiency of the 1.34- $\mu\text{m}$  pump radiation to the second Stokes component was 5% with the slope efficiency equal to 10%. Note that the efficiency of conversion to the first Stokes component was of the same order of magnitude (6%, see Fig. 9b). The total slope efficiency of conversion to the first and second Stokes components was 22%.

The  $\text{Cr}^{2+} : \text{ZnSe}$  laser was pumped by the  $\text{BaWO}_4$  Raman laser. Due to a broad absorption band of the  $\text{Cr}^{2+} : \text{ZnSe}$  crystal, both Stokes components of the Raman laser can be used for pumping. We used in this experiment a

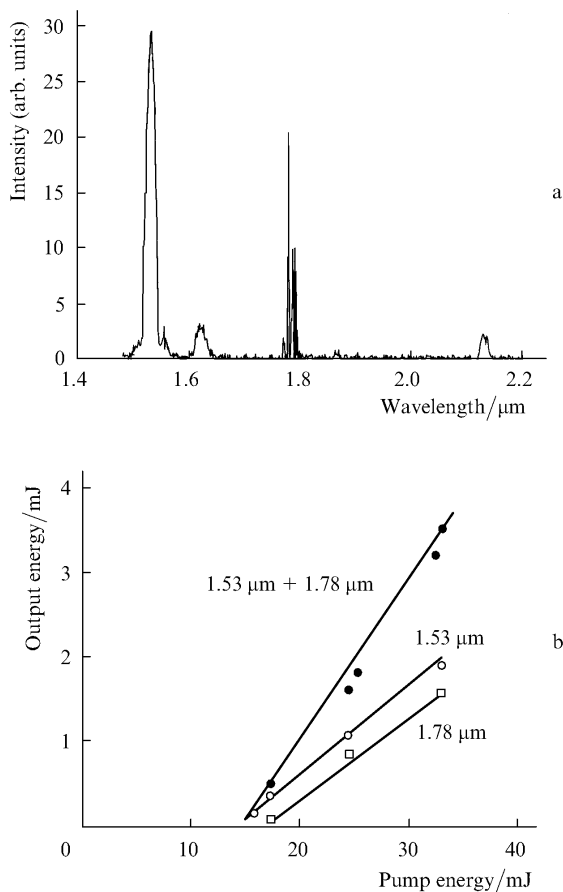


**Figure 9.** Output emission spectrum (a) and the output energy (b) of the  $\text{BaWO}_4$  Raman laser pumped by the 1.34- $\mu\text{m}$  radiation from the  $\text{Nd}^{3+} : \text{YAG}$  laser. The total slope efficiency is 22%.

2.5-mm thick  $\text{Cr}^{2+} : \text{ZnSe}$  crystal absorbing 75% of pump radiation at 1.53  $\mu\text{m}$ . A semi-concentric resonator of this laser of length 40 mm was formed by a spherical input mirror with the radius of curvature  $\rho = 100$  mm and a flat output mirror. The pump radiation was focused into the crystal by a lens with the focal length  $f = 100$  mm, which was placed in front of the spherical mirror. The pump energy was varied using a set of neutral filters.

Figure 10 shows the output parameters of the  $\text{Cr}^{2+} : \text{ZnSe}$  laser for resonators with different reflectivities of the output mirror. One can see that the minimum lasing threshold was 250  $\mu\text{J}$  and the maximum slope efficiency was 11%. The maximum total lasing efficiency for the output mirror with  $R = 34\%$  was 8%. The round-trip passive losses in the resonator were estimated from the Findlay–Clay analysis [33] (Fig. 11a). One can see that the losses per round-trip were 10%. This value is close to losses in a  $\text{Cr}^{2+} : \text{ZnS}$  crystal synthesised using a standard technology. On the other hand, the resonator losses can be estimated from the dependence of the slope efficiency on the reflectivity of the output mirror [36]

$$\frac{1}{\eta} = \frac{1}{\eta_0} \left( 1 + \frac{L_p}{T} \right), \quad (3)$$

where  $\eta$  is the slope efficiency and  $\eta_0$  is the limiting slope efficiency. Losses per round-trip estimated from (3) are 13%. This value is close to losses calculated from the lasing threshold. The difference between the losses can be caused by a greater influence of the nonstationary lasing regime on the slope lasing efficiency than on the lasing threshold.

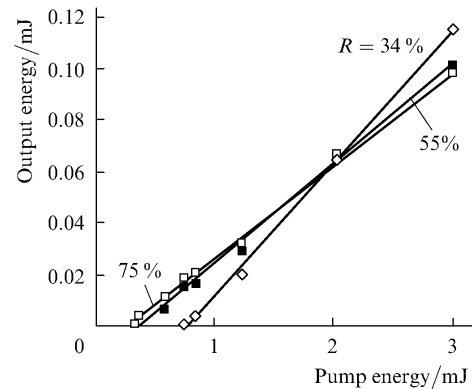


**Figure 10.** Output energy of the  $\text{Cr}^{2+} : \text{ZnSe}$  laser for resonators with different output-mirror reflectivities  $R$ .

We also studied the time delay between the pump and output pulses of the  $\text{Cr}^{2+} : \text{ZnSe}$  laser. The lasing dynamics was measured with a Ge: Au photoresistor cooled down to 77 K and recorded with a Tektronix TDS-380 digital oscilloscope. The time resolution of the detection system determined by the photoresistor was 7 ns. Figure 12 shows the dependences of the time delay between the leading edges of the pump and output pulses for the  $\text{Cr}^{2+} : \text{ZnSe}$  laser with different output mirrors. One can see that the lasing build-up time changed in experiments from 35 to 170 ns depending on the reflectivity of the output mirror and the pump-pulse energy. The time delays observed in experiments are comparable with typical duration of  $Q$ -switched laser

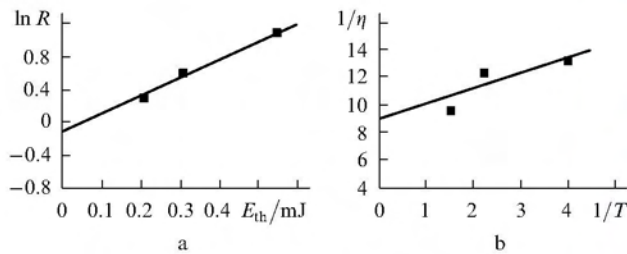


**Figure 11.** Dependences of the lasing threshold of the Cr<sup>2+</sup>:ZnSe laser on the output-mirror reflectivity (a) and of the coefficient  $1/\eta$  on  $1/T$  (b).

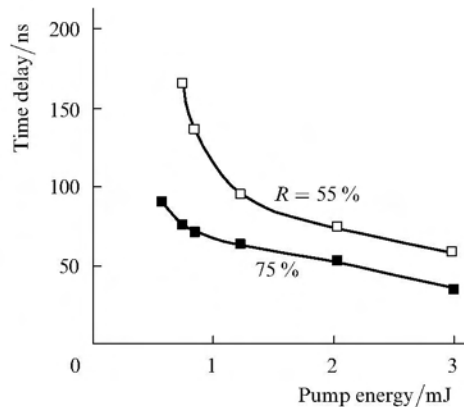


**Figure 12.** Lasing build-up time for the Cr<sup>2+</sup>:ZnSe laser with different output-mirror reflectivities  $R$  as a function of the pump energy.

pulses, exceeding them sometimes. This should be taken into account in possible further nonlinear conversions for obtaining the sum and difference frequency generation by mixing pump radiation with the output radiation from the Cr<sup>2+</sup>:ZnSe (Cr<sup>2+</sup>:ZnS) laser.

## 5. Conclusions

We have studied the spectral and lasing properties of Cr<sup>2+</sup>:ZnS and Cr<sup>2+</sup>:ZnSe crystals synthesised by the chemical transport method followed by the thermal diffusion doping of Cr<sup>2+</sup> ions and pumped by nanosecond laser pulses. We have shown that the maximum slope efficiency of these lasers can achieve 20% and the output pulse can be delayed with respect to the pump pulse by 35–170 ns.

**Acknowledgements.** This work was partially supported by the NSF grants ECS-0140484, ECS-9710428, DMR-0116098, Collaborative Linkage NATO grant PST.CLG.979125, ISTC/EOARD grant 2022P, the Fundamental Spectroscopy Program of the Ministry of Science and Technology of the Russian Federation (M-3-02), and the Program on the Integration of Science and Higher Education of the Russian Federation Government (IO821).

## References

- [1.](#) Pappalardo R., Dietz R.E. *Phys. Rev.*, **123**, 1888 (1961).
- [2.](#) Vallin J.T., Stack G.A., Roberts S. *Phys. Rev. B*, **2** (11), 4313 (1970).
- [3.](#) Kelly C.S., Williams F. *Phys. Rev. B*, **2**, 3 (1970).
- [4.](#) Grebe G., Schulz H.-J. *Zs. Naturforsch.*, **29a**, 1803 (1974).
- [5.](#) Grebe G., Zimmermann H., Schulz H.-J. *Zr. Phys. B*, **91**, 429 (1993).
- [6.](#) Abhvani A.S., Bates C.A., Clerjoud B., Pooler D.R. *J. Phys. C*, **15**, 1345 (1982).
- [7.](#) DeLoach L.D., Page R.H., Wilke G.D., Payne S.A., Krupke W.F. *IEEE J. Quantum Electron.*, **32**, 885 (1996).
- [8.](#) Page R.H., Schaffers K.I., DeLoach L.D., Wilke G.D., Patel F.D., Tassano J.B., Payne S.A., Krupke W.F., Chen K.T., Burger A. *IEEE J. Quantum Electron.*, **33**, 609 (1997).
- [9.](#) Hömmerich U., Wu X., Davis V.R., Trivedi S.B., Grasza K., Chen R.J., Kutcher S. *Opt. Lett.*, **22**, 1180 (1997).
- [10.](#) Graham K., Mirov S.B., Fedorov V.V., Zvanut M.E., Avanesov A., Ignat'ev B., Badikov V.V., Panyutin V., Shevirdyaeva G., in *OSA Trends in Optics and Photonics, Advanced Solid State Lasers* (Washington, DC, Optical Society of America, 2001) Vol. 50, p. 561.
- [11.](#) Mirov S.B., Fedorov V.V., Graham K., Moskalev I.S., Badikov V.V., Panyutin V., Schaffers K.I. *Opt. Lett.*, **27**, 909 (2002).
- [12.](#) Sorokina I.T., Sorokin E., Mirov S., Fedorov V., Badikov V., Panyutin V., Di Lieto A., Tonelli M. *Appl. Phys. B*, **74**, 607 (2002).
- [13.](#) Sorokina I.T., Sorokin E., Mirov S., Fedorov V., Badikov V., Panyutin V., Schaffers K.I. *Opt. Lett.*, **27**, 1040 (2002).
- [14.](#) McKay J., Kraus D., Schepler K.L., in *OSA Trends in Optics and Photonics, Advanced Solid State Lasers* (Washington, DC, Optical Society of America, 2000) Vol. 34, p. 219.
- [15.](#) Hömmerich U., Wu X., Davis V.R., Trivedi S.B., Grasza K., Chen R.J., Kutcher S. *Opt. Lett.*, **22**, 1180 (1997).
- [16.](#) Seo J.T., Hömmerich U., Zong H., Trivedi S.B., Kutcher S.W., Wang C.C., Chen R.J. *Phys. Status Sol.(a)*, **175**, R3 (1999).
- [17.](#) Seo J.T., Hömmerich U., Trivedi S.B., Chen R.J., Kutcher S. *Opt. Commun.*, **153**, 267 (1998).
- [18.](#) Wagner G.J., Carrig T.J., Page R.H., Schaffers K.I., Ndad J.O., Ma X., Burger A. *Opt. Lett.*, **24**, 19 (1999).
- [19.](#) Podlipensky A.V., Shcherbitsky V.G., Kuleshov N.V., Levchenko V.I., Yakimovich V.N., Dening A., Mond M., Kuck S., Huber G., in *OSA Trends in Optics and Photonics, Advanced Solid State Lasers* (Washington, DC, Optical Society of America, 2000) Vol. 34, p. 201.
- [20.](#) Sorokina I.T., Sorokin E., Di Lieto A., Tonelli M., Page R.H., Schaffers K.I., in *OSA Trends in Optics and Photonics, Advanced Solid State Lasers* (Washington, DC, Optical Society of America, 2000) Vol. 34, p. 188.
- [21.](#) Sennaroglu A., Konea A.O., Pollock C.R., in *OSA Trends in Optics and Photonics, Advanced Solid State Lasers* (Washington, DC, Optical Society of America, 2000) Vol. 34, p. 240.
- [22.](#) Podlipensky A.V., Shcherbitsky V.G., Kuleshov N.V., Mikhailov V.P., Levchenko V.I., Yakimovich V.N., Postnova L.I., Konstantinov V.I. *Opt. Commun.*, **167**, 129 (1999).
- [23.](#) Carrig T.J., Wagner G.J., Sennaroglu A., Jeong J.Y., Pollock C.R., in *OSA Trends in Optics and Photonics, Advanced Solid State Lasers* (Washington, DC, Optical Society of America, 2000) Vol. 34, p. 182.
- [24.](#) Carrig T.J., Wagner G.J., Sennaroglu A., Jeong J.Y., Pollock C.R. *Opt. Lett.*, **25**, 168 (2000).
- [25.](#) Sorokina I.T., Sorokin E., Di Lieto A., Tonelli M., Page R.H., Schaffers K.I. *Tech. Dig. Conf. on Advanced Solid State Lasers* (Washington, DC, Optical Society of America, 2001) pp 87–89.
- [26.](#) Page R.H., Skidmore J.A., Schaffers K.I., Beach R.J., Pane S.A., Krupke W.F., in *OSA Trends in Optics and Photonics, Advanced Solid State Lasers* (Washington, DC, Optical Society of America, 1997) Vol. 10, p. 208.
- [27.](#) Podlipensky A.V., Shcherbitsky V.G., Kuleshov N.V., Levchenko V.I., Yakimovich V.N., Mond M., Heumann E., Huber G., Kretschmann H., Kuck S. *Appl. Phys. B*, **72**, 253 (2001).
- [28.](#) Sorokina I.T., Sorokin E., Page R.H. *Tech. Dig. Conf. on Advanced Solid State Lasers* (Washington, DC, Optical Society of America, 2001) p. 51.
- [29.](#) Nikogosian D.N. *Properties of Optical and Laser-Related Materials: a Handbook* (England: John Wiley&Sons, 1997).
- [30.](#) Hartmann H. *J. Crystal Growth*, **42**, 144 (1977).

- [doi>](#) 31. Shcherbitsky V.G., Girard S., Fromager M., Moncorge R., Kuleshov N.V., Levchenko V.I., Yakimovich V.N., Ferrand B. *Appl. Phys. B*, **74**, 367 (2002).
- [doi>](#) 32. Burger A., Chattopadhyay K., Ndap J.-O., Ma X., Morgan S.H., Rablau C.J., Su C.H., Feth S., Page R.H., Schaffers K.L., Pane S.A. *J. Crystal Growth*, **225**, 249 (2002).
- [doi>](#) 33. Findlay D., Clay R.A. *Phys. Lett.*, **20**, 277 (1966).
- 34. Basiev T.T., Doroshenko M.E., Zverev P.G., Prokhorov A.M., RF Patent No. 217893C1, 25.04.00.
- [doi>](#) 35. Zverev P.G., Basiev T.T., Sobot' A.A., Skorniyakov V.V., Ivleva L.I., Polozkov N.M., Osiko V.V. *Kvantovaya Elektron.*, **30**, 55 (2000) [*Quantum Electron.*, **30**, 55 (2000)].
- [doi>](#) 36. Caird J.A., Payne S.A., Staver P.R., Ramponi A.J., Chase L.L., Krupke W.F. *IEEE J. Quantum Electron.*, **24**, 1077 (1988).